JPE 16-4-22

http://dx.doi.org/10.6113/JPE.2016.16.4.1469
ISSN(Print): 1598-2092 / ISSN(Online): 2093-4718

A Modularized Equalizer for Supercapacitor Strings in Hybrid Energy Storage Systems

Zhigang Gao† and Fenlin Jiang*

†,*School of Automation, Beijing Institute of Technology, Beijing, China

Abstract

In hybrid energy storage systems, supercapacitors are usually connected in series to meet the required voltage levels. Equalizers are effective in prolonging the life of hybrid energy storage systems because they eliminate the voltage imbalance on cells. This study proposes a modularized equalizer, which is based on a combination of a half-bridge inverter, an inductor, and two auxiliary capacitors. The proposed equalizer inherits the advantages of inductor-based equalization systems, but it also offers unique merits, such as low switching losses and an easy-to-use control algorithm. The zero-voltage switching scheme is analyzed, and the power model is established. A fixed-frequency operation strategy is proposed to simplify the control and lower the cost. The switching patterns and conditions for zero-voltage switching are discussed. Simulation results based on PSIM are presented to verify the validity of the proposed equalizer. An equalization test for two supercapacitor cells is performed. An experimental hybrid energy storage system, which consists of batteries and supercapacitors, is established to verify the performance of the proposed equalizer. The analysis, simulation results, and experimental results are in good agreement, thus indicating that the circuit is practical.

Key words: Equalization system, Equalizer, Pulse width modulation (PWM), Storage system, Supercapacitor, Zero-voltage switching (ZVS)

I. INTRODUCTION

As a result of the requirements for mass energy storage in power systems and other applications, numerous types of elements for energy storage have been developed. In particular, supercapacitors (SCs) are widely used in electric vehicles/elevators, in which the motor accelerates and decelerates frequently, or in power systems for voltage regulation and system optimization [1]-[8]. The voltage of each SC cell is relatively low (2.7 V or 5.5 V typically), and generally, SC cells are connected in series to meet the voltage requirements in industrial applications.

The characteristics of SC cells, including their resistance and capacitance, tend to differ because of manufacturing techniques, architectures, and degradation. Thus, overcharging and over discharging are likely to occur and thereby cause serious overheating, shorten the lifetime of systems, and ultimately corrupt the strings. Hence, equalizers for balancing the voltages of all cells should be introduced. Different types of equalizers have been presented [9]-[32].

Typically, equalization methods come in two types: energy-consuming and energy-transferring equalization methods. The former method consumes the excess energy on specific cells by using resistors. This type of equalization system is easy to establish. However, excess energy is wasted, and such waste may increase string temperature and reduce reliability. In addition, the limitations of resistors restrict the response time of this equalization method.

The energy-transferring method can provide additional power flow paths for different cells and transfer the excess energy from one cell to another. For example, when the SC string is charging, the equalizer transfers the energy from the cell with a high voltage to the cell with a low voltage. Thus, the voltages of all cells can be balanced. Different types of elements, such as inductors, capacitors, and transformers can be used as buffers. Unlike the energy-consuming method, the energy-transferring method does not waste excess energy but instead transfers it to the cells lacking energy. Therefore, the efficiency and reliability of systems are improved, and string lifetime is prolonged.

Fig. 1 shows some typical equalizers and is divided into

Manuscript received Dec. 19, 2015; accepted Mar. 7, 2016
Recommended for publication by Associate Editor Jonghoon Kim.
†Corresponding Author: gzg@bit.edu.cn
Tel: +86-13466772534, Beijing Institute of Technology
*School of Automation, Beijing Institute of Technology, China

© 2016 KIPE

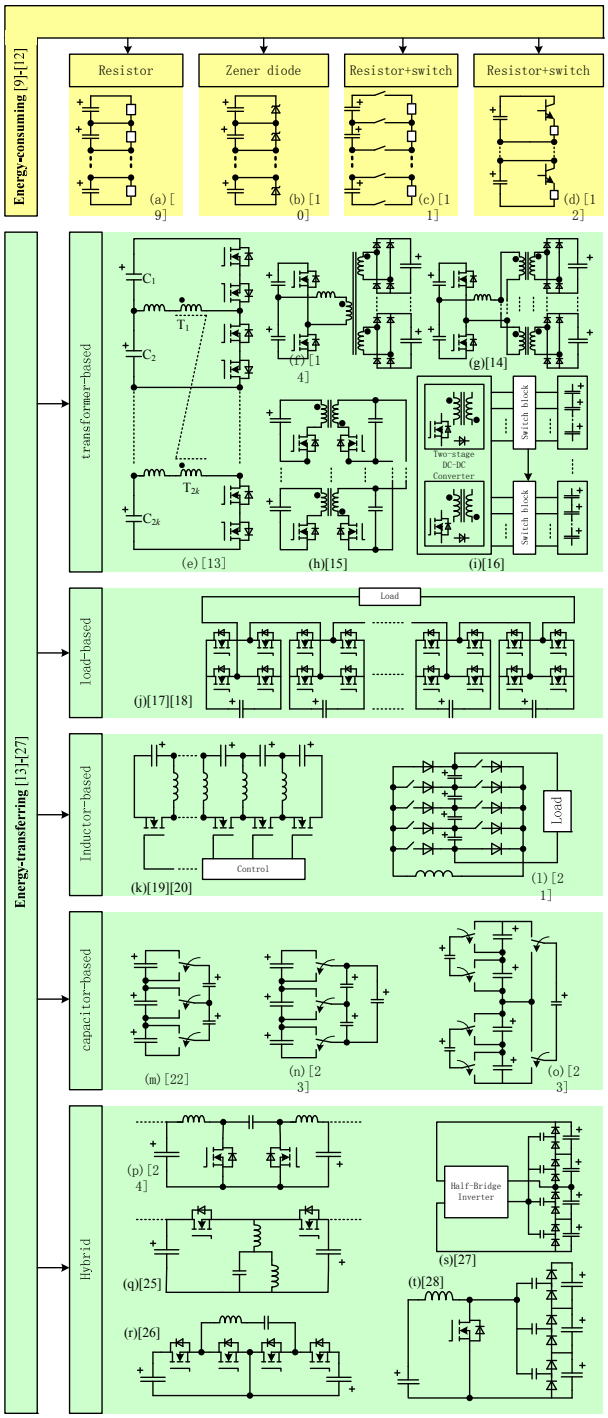

Fig. 1. Overview of the equalizers. (a) Based on resistors, (b) Based on Zener diodes, (c) Based on resistors and switches, (d) Based on resistors and transistors, (e) Based on multi-winding transformers and bi-directional switches, (f) Based on single bridge multi-winding transformers, (g) Based on single bridge multi-transformers, (h) Based on fly-back converters, (i) Based on two-stage DC-DC converters, (j) Based on cascaded H-bridge converters, (k) Based on multiple inductors, (l) Based on a single inductor, (m) Based on capacitors, (n) Based on double-tiered capacitors, (o) Based on triple-tiered capacitors, (p) Based on Cuk converters, (q) Based on quasi-resonant zero-current switching converter, (r) Resonant switched-capacitor cell-balancing system, (s) Based on half-bridge inverters, and (t) Based on boost inverters.

two groups. Figs. 1(a)–1(d) are based on the energy-consuming method. The resistors and Zener diodes are selected to connect in parallel to the SC cells to consume the excess energy [9]-[12]. The method can be used in cases of small capacity because of its low cost and simplicity.

Several types of topologies exist, and they are based on the different elements that function as buffers for the energy-transferring method [13]-[28].

Transformers are adopted in the circuits shown in Figs. 1(e)–1(i). High-/Middle-frequency techniques are often introduced to reduce the size and weight of the transformers. In [13], bi-directional switches and a multi-winding transformer are used to form an equalizer, as shown in Fig. 1(e). In [14], a single-bridge converter is used to charge all the SC cells through a multi-winding transformer or several two-winding transformers, as shown in Figs. 1(f)–1(g). As the voltage drop of the diode rectifier is about 1 V, the efficiency of the converter is low, and the energy cannot flow from one cell to another. In [15], several DC/DC converters based on high-frequency transformers are introduced to charge the cells in the string, as shown in Fig. 1(h); such string is complicated and difficult to control. A similar topology is shown in Fig. 1(i) and discussed in [16]. Some converters are introduced to maintain cell voltages.

An equalizer based on cascaded H-bridge converters is proposed in [17], [18]. Each SC string serves as the DC power of the H-bridge, and the outputs are connected in series. By adjusting the reference voltage of each cell, the charging/discharging power can be controlled, and the voltages can be balanced. The performance of the equalizer is affected by the load current, and the equalizer cannot work when the system is open-circuit, as shown in Fig. 1(j).

Inductors are introduced to transfer energy from one cell to another, as shown in [19], [20]. Fig. 1(k) shows the topologies in detail. At first, the energy is stored in the inductor and then transferred into the adjacent cells. Thus, several inductors are set between every two cells. In [21], a single inductor is used to store energy, which can then flow into other cells through the switches, as shown in Fig. 1(l).

In [12], capacitors are introduced to balance voltages, as shown in Fig. 1(m). At first, the energy is transferred into the capacitors. It then flows into the cells that lack energy. In [23], [24], additional switches and capacitors are installed to provide other routines that can shorten equalization time, as shown in Figs. 1(n) and 1(o).

Hybrid equalization systems are formed on the basis of the different types of elements, as shown in Figs. 1(p)–1(t). In [24], an equalizer derived from the Cuk converter is proposed, as shown in Fig. 1(p). Power can flow from one cell to an adjacent cell. Fig. 1(q) shows an equalization topology introduced in [25], in which one inductor and one capacitor work together to store and release the energy. In this way, quasi-resonant zero-current switching, which can reduce

switching losses, is realized. A similar equalizer is shown in Fig. 1(r), and the operation scheme is introduced in [26]. Other equalization circuits are based on the different types of converters, such as half-bridge inverters [27] and boost converters [28] (Figs. 1(s) and (t)). These topologies are effective, but they lack modularity.

Manufacturing transformers is difficult, and the topology is not highly modularized. Load-based equalization circuits are simple, but they can only be used in certain applications. In inductor-based and capacitor-based equalization circuits, the parameters need not be precise, and the topology need not be highly modularized. In hybrid equalization circuits, soft-switching techniques can be applied to further reduce switching losses.

For these reasons, the present study proposes a modularized equalizer with zero-voltage switching (ZVS) and applies this equalizer to an SC string. This structure of the proposed equalization circuit is similar to the topology introduced in [19] (Fig. 1(k)). However, additional capacitors are employed to realize ZVS. As a result of its modularity, the proposed topology can be expanded. This design inherits the advantages of inductor-based topologies, overcomes the disadvantages of transformer-based topologies, and facilitates the expansion of equalization systems. ZVS is realized, and switching losses are consequently reduced. These conditions promote the increase in switching frequency, reduce the size of inductors, and prolong the lifetime of SC strings.

The proposed equalization circuit is analyzed in this work. A modularized control scheme is established. Simulation and experimental results are shown to verify the performance of the topology.

II. Proposed Topology of Equalizer

The equalizer proposed in this work is shown in Fig. 2. The string is made up of N SC cells, i.e., SC-1–SC-N. Their voltages are $U_{SC\text{-}1}$–$U_{SC\text{-}N}$.

For every two adjacent SC cells, an equalizer is added to carry out equalization. As shown in Fig. 2, module-k is for SC-k and SC-(k+1), where k = 1, 2..., N−1. Every module consists of two switches, two auxiliary capacitors, and one inductor. For simplicity, all the inductors shown in Fig. 2 are equal to L, and all the capacitors are equal to C. The MOSFETs are labeled as K_1–$K_{2N\text{-}2}$.

The equalization system proposed in this work exhibits the following special features.

(1) The equalizer is based on several independent modules, the parameters of which are identical. Thus, the system is highly modularized, and the equalization system for different applications can be easily modified.

(2) ZVS can be achieved with auxiliary capacitors and inductors. Switching losses can be reduced, and the lifetime of the string is prolonged.

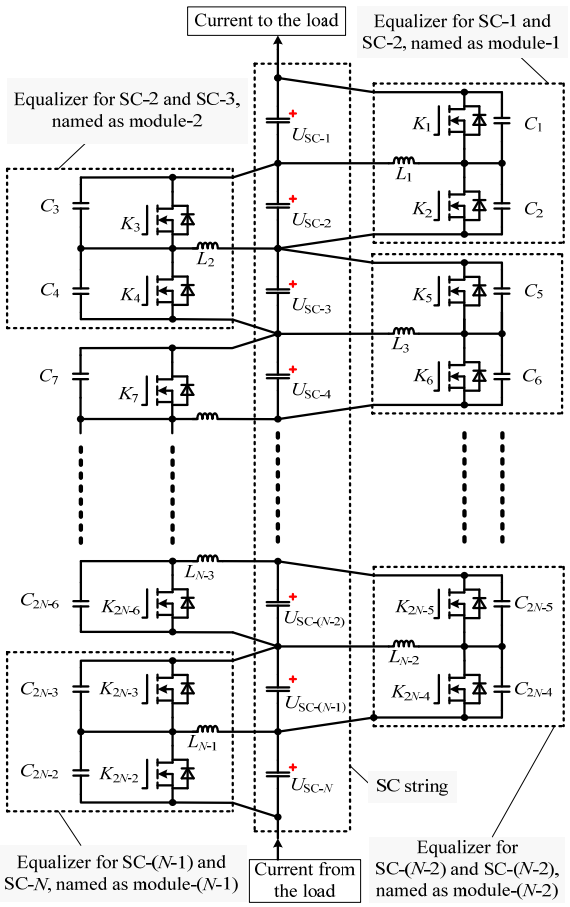

Fig. 2. Topology of the proposed equalizer.

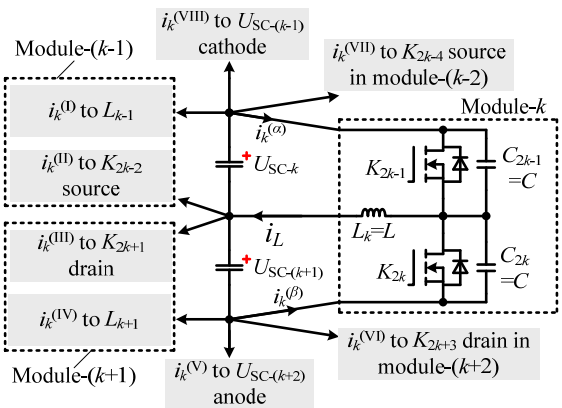

Fig. 3. Topology of module-k.

(3) All the modules are independent and utilize the same control schemes. The control algorithm is easy to realize with digital processors, and its cost is low.

III. Equalization System Analysis

A. Analysis of module-k

In Fig. 2, module-k is the equalizer for SC-k and SC-(k+1), where k = 1, 2, 3..., N−1. The topology of module-k is redrawn in Fig. 3. $i_k^{(I)}$–$i_k^{(VIII)}$ represent the currents flowing to the different parts of the system. $i_k^{(\alpha)}$, $i_k^{(\beta)}$, and i_L are the

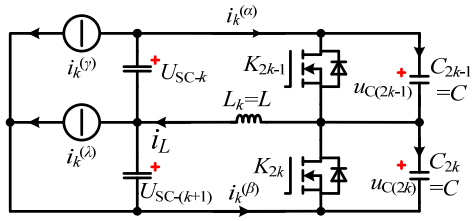

Fig. 4. Equivalent circuit of module-k.

currents flowing into module-k.

Based on Kirchhoff's current law, the currents in Fig. 3 can be calculated as

$$\begin{cases} i_k^{(\alpha)} + i_k^{(\beta)} = i_L \\ i_k^{(\gamma)} \equiv i_k^{(\mathrm{I})} + i_k^{(\mathrm{VII})} + i_k^{(\mathrm{VIII})} \\ i_k^{(\lambda)} \equiv i_k^{(\mathrm{II})} + i_k^{(\mathrm{III})} \end{cases} \tag{1}$$

The equivalent circuit of module-k is shown in Fig. 4.

In Fig. 4, L is the inductance, and i_L is the current on the inductor. The voltages of the two SC cells are denoted by $U_{SC\text{-}k}$ and $U_{SC\text{-}(k+1)}$. $K_{2k\text{-}1}$ and K_{2k} are the two MOSFETs. $C_{2k\text{-}1}$ and C_{2k} are the auxiliary capacitors, which are used to realize ZVS. Their voltages are denoted by $u_{C(2k\text{-}1)}$ and $u_{C(2k)}$. $i_{C(2k\text{-}1)}$ and $i_{C(2k)}$ are the currents flowing into the two auxiliary capacitors.

Module-k works as follows.

[STAGE 1]: The analysis begins at $t = t_1$ when $K_{2k\text{-}1}$ is turned on, K_{2k} is turned off, and $i_L = 0$. The equivalent circuit is shown in Fig. 5. The state equations are

$$\begin{cases} u_{C(2k\text{-}1)}(t) = 0 \\ u_{C(2k)}(t) = U_{SC\text{-}k} + U_{SC\text{-}(k+1)} \\ L\dfrac{\mathrm{d}i_L(t)}{\mathrm{d}t} = U_{SC\text{-}k} \Rightarrow i_L(t) = \dfrac{U_{SC\text{-}k}(t-t_1)}{L} \end{cases} \quad t_1 \le t < t_2 \tag{2}$$

[STAGE 2]: After t_2, $K_{2k\text{-}1}$ and K_{2k} are both turned off. $\Delta \equiv t_2 - t_1$ is employed to represent the time span between t_1 and t_2. The equivalent circuit is shown in Fig. 6. The state equations are shown in (3), where $u_{C(2k\text{-}1)}(t_2) = 0$, $u_{C(2k)}(t_2) = U_{SC\text{-}k}+U_{SC\text{-}(k+1)}$, and $i_L(t_2) = \Delta U_{SC\text{-}k}/L$.

$$\begin{cases} u_{C(2k-1)}(t) + L\dfrac{\mathrm{d}i_L(t)}{dt} = U_{SC\text{-}k} \\ u_{C(2k)}(t) - L\dfrac{\mathrm{d}i_L(t)}{dt} = U_{SC\text{-}(k+1)} \\ C\dfrac{\mathrm{d}u_{C(2k\text{-}1)}(t)}{\mathrm{d}t} - C\dfrac{\mathrm{d}u_{C(2k)}(t)}{\mathrm{d}t} = i_L(t) \end{cases} \quad t_2 \le t < t_3 \tag{3}$$

The solutions are shown in (4), where $t_2 \le t < t_3$.

$$\begin{cases} u_{C(2k-1)}(t) = U_{SC\text{-}k} - U_{SC\text{-}k}\cos(\omega t - \omega t_2) \\ \qquad + \Delta U_{SC\text{-}k}\omega \sin(\omega t - \omega t_2) \\ u_{C(2k)}(t) = U_{SC\text{-}(k+1)} + U_{SC\text{-}k}\cos(\omega t - \omega t_2) \\ \qquad - \Delta U_{SC\text{-}k}\omega \sin(\omega t - \omega t_2) \\ i_L(t) = \dfrac{\Delta U_{SC\text{-}k}}{L}\cos(\omega t - \omega t_2) + \dfrac{U_{SC\text{-}k}}{\omega L}\sin(\omega t - \omega t_2) \end{cases} \tag{4}$$

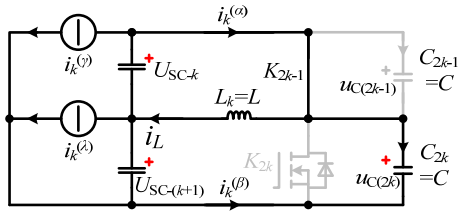

Fig. 5. Equivalent circuit when $t_1 \le t < t_2$ or $t_6 \le t < t_7$.

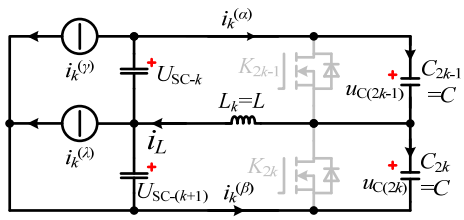

Fig. 6. Equivalent circuit when $t_2 \le t < t_3$ or $t_5 \le t < t_6$.

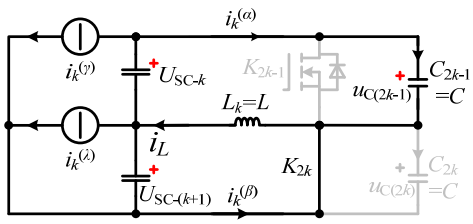

Fig. 7. Equivalent circuit when $t_3 \le t < t_4$ or $t_4 \le t < t_5$.

ω is the resonant angular frequency and is defined as

$$\omega = \frac{1}{\sqrt{2LC}} \tag{5}$$

At t_3, $u_{C(2k)} = 0$, and $u_{C(2k\text{-}1)} = U_{SC\text{-}k}+U_{SC\text{-}(k+1)}$. After t_3, the parasitic diode conducts automatically, and K_{2k} can be turned on. As $u_{C(2k)} = 0$, ZVS can be realized. Moreover, t_3 can be calculated as

$$\sin(\omega t_3 - \omega t_2 - \varphi_1) = \frac{\sigma}{\sqrt{1+\Delta^2\omega^2}} \tag{6}$$

where φ_1 is the initial phase that can be written as (7). σ is defined as (8), which is the ratio of the two SC cell voltages.

$$\cos(\varphi_1) = \frac{\Delta\omega}{\sqrt{1+\Delta^2\omega^2}} \tag{7}$$

$$\sigma = \frac{U_{SC\text{-}(k+1)}}{U_{SC\text{-}k}} \tag{8}$$

In this stage, $u_{c(2k\text{-}1)}$ rises from 0 to $U_{SC\text{-}k}+U_{SC\text{-}(k+1)}$, whereas $u_{c(2k)}$ falls from $U_{SC\text{-}k}+U_{SC\text{-}(k+1)}$ to 0. Considering $U_{SC\text{-}k} = U_{SC\text{-}(k+1)}$, we obtain the following:

$$\begin{aligned} &\frac{1}{C}\int_{t_2}^{t_3} i_k^{(\alpha)}dt + \frac{1}{C}\int_{t_2}^{t_3}(-i_k^{(\beta)})dt = 0 \\ &\Rightarrow \int_{t_2}^{t_3} U_{SC-k} i_k^{(\alpha)}dt \approx \int_{t_2}^{t_3} U_{SC-(k+1)} i_k^{(\beta)}dt \end{aligned} \tag{9}$$

The energy stored in the two auxiliary capacitors at t_2 and t_3 is the same. Thus,

$$i_L(t_2) \approx i_L(t_3) \tag{10}$$

[STAGE 3]: The equivalent circuit after t_3 is shown in Fig. 7. The state equations are presented in (11), where $t_3 \le t < t_4$.

$$\begin{cases} u_{C(2k\text{-}1)}(t) = U_{SC\text{-}k} + U_{SC\text{-}(k+1)} \\ u_{C(2k)}(t) = 0 \\ L\dfrac{di_L(t)}{dt} = -U_{SC\text{-}(k+1)} \Rightarrow i_L(t) = -\dfrac{U_{SC\text{-}(k+1)}(t-t_3)}{L} \end{cases} \tag{11}$$

At t_4, i_L falls to zero. With (2), (10), and (11), we can calculate t_4–t_3 as

$$t_4 - t_3 = \frac{i_L(t_3)L}{U_{SC-(k+1)}} \approx \frac{i_L(t_2)L}{U_{SC-(k+1)}} \approx \Delta \tag{12}$$

[STAGE 4]: The equivalent circuit after t_4 is shown in Fig. 7. $\Gamma \equiv t_5 - t_4$ is employed to represent the time span between t_4 and t_5. At the end of the stage, $u_{C(2k\text{-}1)}$ is $U_{SC\text{-}k}+U_{SC\text{-}(k+1)}$, $u_{C(2k)}$ is 0, and i_L is $-\Gamma U_{SC\text{-}(k+1)}/L$.

[STAGE-5]: After t_5, $K_{2k\text{-}1}$ and K_{2k} are both turned off. The equivalent circuit is shown in Fig. 6. For $t_5 \le t < t_6$, the solutions are

$$\begin{cases} u_{C(2k-1)}(t) = U_{SC\text{-}k} + U_{SC\text{-}(k+1)}\cos(\omega t - \omega t_5) \\ \qquad\qquad -\Gamma U_{SC\text{-}(k+1)}\omega\sin(\omega t - \omega t_5) \\ u_{C(2k)}(t) = U_{SC\text{-}(k+1)} - U_{SC\text{-}(k+1)}\cos(\omega t - \omega t_5) \\ \qquad\qquad +\Gamma U_{SC\text{-}(k+1)}\omega\sin(\omega t - \omega t_5) \\ i_L(t) = -\dfrac{\Gamma U_{SC\text{-}(k+1)}}{L}\cos(\omega t - \omega t_5) - \dfrac{U_{SC\text{-}(k+1)}}{\omega L}\sin(\omega t - \omega t_5) \end{cases} \tag{13}$$

At t_6, $u_{C(2k\text{-}1)}$ falls to 0, and $K_{2k\text{-}1}$ is turned on. t_6 can be obtained with (14), where φ_2 is defined in (15).

$$\sin(\omega t_6 - \omega t_5 - \varphi_2) = \frac{1}{\sigma\sqrt{1+\Gamma^2\omega^2}} \tag{14}$$

$$\cos(\varphi_2) = \frac{\Gamma\omega}{\sqrt{1+\Gamma^2\omega^2}} \tag{15}$$

[STAGE 6]: The equivalent circuit after t_6 is shown in Fig. 5. The state equations are presented in (16), where $t_6 \le t < t_7$.

$$\begin{cases} u_{C(2k)}(t) = U_{SC\text{-}k} + U_{SC\text{-}(k+1)} \\ u_{C(2k\text{-}1)}(t) = 0 \\ L\dfrac{di_L(t)}{dt} = U_{SC\text{-}k} \Rightarrow i_L(t) = \dfrac{U_{SC\text{-}k}(t-t_6)}{L} \end{cases} \tag{16}$$

At t_7, i_L falls to zero, and another cycle starts. Similar to that in [STAGE 3], t_7–t_6 can be calculated as

$$t_7 - t_6 \approx \Gamma \tag{17}$$

Fig. 8 shows the voltages and current in an entire cycle. Table I shows the switching states from t_1 to t_7. In every cycle, ZVS for K_1 and K_2 is realized.

B. Conditions for ZVS

At t_3, if $u_{C(2k)}(t_3) = 0$ and $i_L(t_3) \ge 0$, the ZVS of K_{2k} can be realized, as shown in Fig. 8. From (6), (7), and (8), the result can be written as

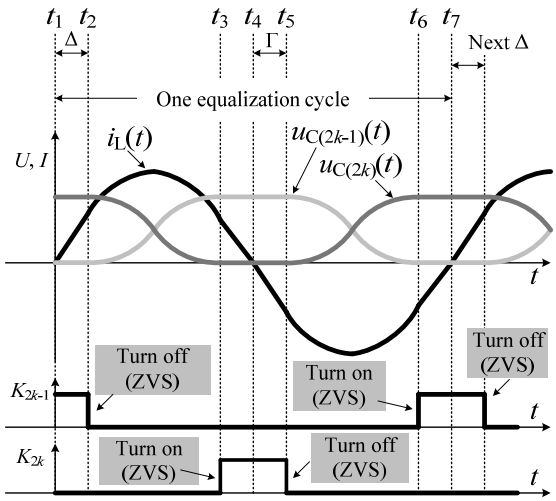

Fig. 8. Current and voltage waveforms in one cycle.

TABLE I
SWITCHING STATES IN ONE CYCLE

Time	$K_{2k\text{-}1}$	K_{2k}
(t_1, t_2)	On	Off
t_2	Turn off (ZVS)	Off
(t_2, t_3)	Off	Off
t_3	Off	Turn on (ZVS)
(t_3, t_4)	Off	On
t_4	Off	On
(t_4, t_5)	Off	On
t_5	Off	Turn off (ZVS)
(t_5, t_6)	Off	Off
t_6	Turn on (ZVS)	Off
(t_6, t_7)	On	Off

$$\sigma \le 1 + (\Delta\omega)^2 \tag{18}$$

Thus, the ZVS condition for K_{2k} is

$$\Delta^2 \ge \frac{\sigma - 1}{\omega^2} \tag{19}$$

The surface described in (19) is drawn in Fig. 9. Noticeably, if $\sigma \le 1$, K_{2k} can always work in ZVS mode. In other words, $U_{SC\text{-}k} \ge U_{SC\text{-}(k+1)}$ is the sufficient condition for the ZVS of K_{2k}; otherwise, (19) must be met.

A similar analysis can be carried out, and the ZVS condition for $K_{2k\text{-}1}$ is

$$\Gamma^2 \ge \frac{\left(\dfrac{1}{\sigma}\right) - 1}{\omega^2} \tag{20}$$

The surface described in (20) can be drawn in Fig. 10. $K_{2k\text{-}1}$ can always work in ZVS mode when $\sigma \ge 1$. In other words, $U_{SC\text{-}(k+1)} \ge U_{SC\text{-}k}$ is the sufficient condition for the ZVS of $K_{2k\text{-}1}$; otherwise, (20) must be satisfied.

C. Power Model of Module-k

In Fig. 8, t_1–t_7 define one cycle for the equalization system.

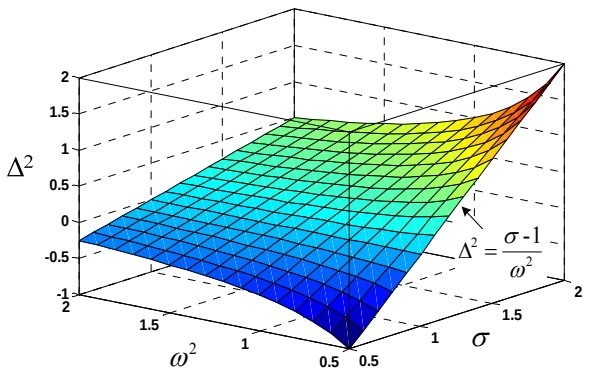

Fig. 9. ZVS conditions for K_{2k}.

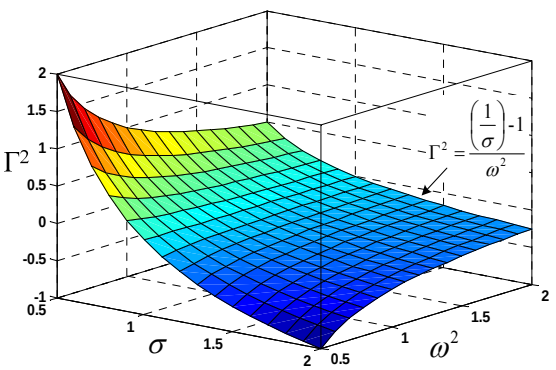

Fig. 10. ZVS conditions for K_{2k-1}.

W_k and W_{k+1} are employed to represent the energy released by SC-k and SC-(k+1) because of module-k in one cycle.

$$W_k = \int_{t_1}^{t_2} U_{\text{SC-}k} i_k^{(\alpha)}(t)dt = \frac{U_{\text{SC-}k}^2(\Delta^2 - \Gamma^2)}{2L} \quad (21)$$

$$W_{k+1} = -\int_{t_1}^{t_2} U_{\text{SC-}(k+1)} i_k^{(\beta)}(t)dt = \frac{U_{\text{SC-}(k+1)}^2(\Gamma^2 - \Delta^2)}{2L} \quad (22)$$

From (21) and (22), we know that the power released by the two SCs is changed by Cell-k. The difference $\hat{W_k}$ is given by

$$\hat{W_k}(\Delta,\Gamma) = W_k - W_{k+1} \approx \frac{U_{\text{SC-}k}^2(\Delta^2 - \Gamma^2)}{L} \quad (23)$$

and

$$\frac{\partial \hat{W_k}(\Delta,\Gamma)}{\partial \Delta} > 0, \quad \frac{\partial \hat{W_k}(\Delta,\Gamma)}{\partial \Gamma} < 0 \quad (24)$$

Hence, increasing Δ or decreasing Γ can transfer the energy from SC-k to SC-(k+1), whereas decreasing Δ or increasing Γ can transfer energy from SC-(k+1) to SC-k.

D. Power Model of the SC Cells in the String

For every SC (SC-k) in the string, the energy stored in it can be changed by three factors:

- Factor 1: The current on the load, which is determined by the load and cannot be changed.
- Factor 2: By (22), that is, the energy flowing out because of module-(k-1) is $\frac{U_{\text{SC-}k}^2(\Gamma_{k-1}^2 - \Delta_{k-1}^2)}{2L}$, where Δ_{k-1} represents Δ introduced in (4) and Γ_{k-1} represents Γ introduced in (10) for module-(k-1).
- Factor 3: By (21), that is, the energy flowing out because of module-k is $\frac{U_{\text{SC-}k}^2(\Delta_k^2 - \Gamma_k^2)}{2L}$, where Δ_k represents Δ introduced in (4) and Γ_k represents Γ introduced in (10) for module-k.

Hence, in the SC string, the energy flowing out of SC-k caused by the equalization system can be written as $\frac{U_{\text{SC-}k}^2[(\Delta_k^2 - \Delta_{k-1}^2) - (\Gamma_k^2 - \Gamma_{k-1}^2)]}{2L}$.

E. Operation Strategy

For every module in the equalization system, the operation strategy can be described as follows:

- If $U_{\text{SC-}k} = U_{\text{SC-}(k+1)}$, then equalization is not necessary. In such a case, all the switches are turned off. In the present work, when $|U_{\text{SC-}k} - U_{\text{SC-}(k+1)}| < 0.2$ V, the two voltages are considered to be equal.
- If $U_{\text{SC-}k} > U_{\text{SC-}(k+1)}$, then Δ is positive, and Γ is set as 0. Then, the power flows from SC-k to SC-(k+1). In such a case, according to (19), K_{2k} can always realize ZVS, and the minimal value of Δ can be obtained. From (2), the maximal value of Δ can be calculated as (25), where $I_{\max}$ is the maximal current allowed in the equalization system.

$$\frac{U_{SC-k}\Delta}{L} \le I_{\max} \Rightarrow \Delta \le \frac{LI_{\max}}{U_{SC-k}} \quad (25)$$

- If $U_{\text{SC-}k} < U_{\text{SC-}(k+1)}$, then Γ is positive, and Δ is set to 0. Then, the power flows from SC-(k+1) to SC-k. In such a case, according to (20), K_{2k-1} can always realize ZVS, and the minimal value of Γ can be obtained. From (11), the maximal value of Γ can be calculated as

$$\frac{U_{SC-(k+1)}\Gamma}{L} \le I_{\max} \Rightarrow \Gamma \le \frac{LI_{\max}}{U_{SC-(k+1)}} \quad (26)$$

When the equivalent resistance in the circuit is considered, the minimal value of Δ or Γ, denoted by ε, should be set to make sure both switches can realize ZVS. That is,

$$\Delta, \Gamma \ge \varepsilon \quad (27)$$

Thus, the operation strategy can be drawn in Fig. 11.

The flow chart shown in Fig. 11 presents three branches. When the two voltages are almost equal (for example, the difference is 0.1 V), the switches are turned off because equalization in such a case is not necessary. Otherwise, the left branch is chosen when the upper capacitor voltage is high, and the right branch is chosen when the upper capacitor voltage is low.

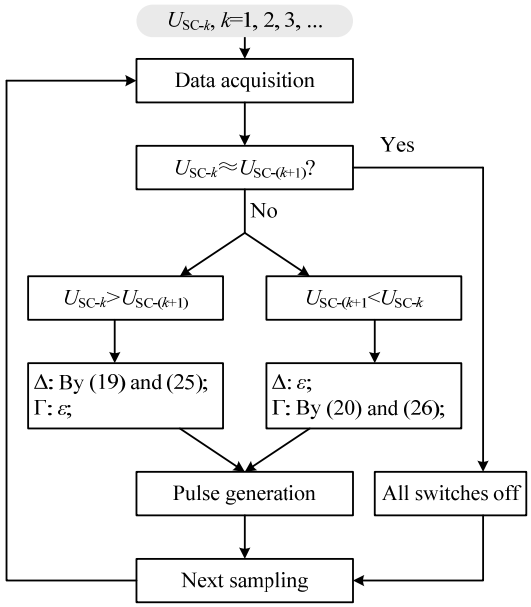

Fig. 11. Flow chart of operation strategy.

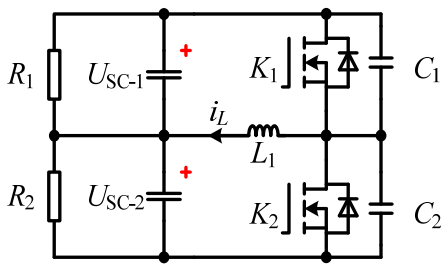

Fig. 12. Equivalent circuit of the simulation system.

IV. Simulation Results

The simulation system for module-1 shown in Fig. 2 is established in PSIM6.0. Two 1 F capacitors $U_{SC\text{-}1}$ and $U_{SC\text{-}2}$ are connected in series. Two MOSFETs are controlled by a DLL block written in C language. The simulation mainly focuses on the verification of the equalizer and the theory proposed in Section III. The equivalent circuit of the simulation topology is shown in Fig. 12.

The parameters of the simulation system are shown in Table II. In Table II, the resistance of L_1 is used to represent the equivalent resistance in the circuit. Given that the initial voltage of C_1 is 0, the initial state of the simulation system is similar to that shown in Fig. 5, in which the equalizer starts from t_1.

The maximal current is set to 3 A. From (25) and (26), we can set Δ, Γ ≤ 120 μs. When the equivalent resistance of the circuit is not considered, Δ and Γ can be

$$\begin{cases} \text{if } U_{SC-1} > U_{SC-2} : \Delta = 110\text{us}, \Gamma = 0 \\ \text{if } U_{SC-1} < U_{SC-2} : \Gamma = 110\text{us}, \Delta = 0 \end{cases} \tag{28}$$

The results are shown in Fig. 13. As a result of the equivalent resistance of the circuit, u_{C1} cannot drop to 0, and

TABLE II
Parameters of the Simulation System

Name	Value
Initial voltage of $U_{SC\text{-}1}$	5.1 V
Initial voltage of $U_{SC\text{-}2}$	4.9 V
Load of $U_{SC\text{-}1}$, R_1	51 Ω
Load of $U_{SC\text{-}2}$, R_2	25.5 Ω
Inductance of L_1	200 μH
Resistance of L_1	0.5 Ω
Initial current of L_1	0
Initial voltage of C_1	0
Capacitance of C_1	10 μF
Initial voltage of C_2	10 V
Capacitance of C_2	10 μF

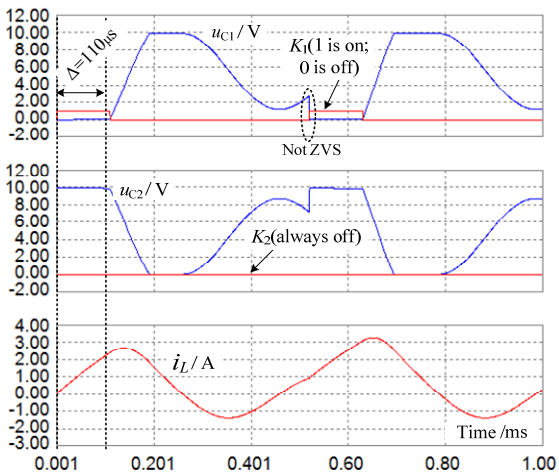

Fig. 13. Simulation results for module-1. (Δ = 110 μs, Γ = 0 μs when $U_{SC\text{-}1} > U_{SC\text{-}2}$; Δ = 0 μs, Γ = 110 μs when $U_{SC\text{-}1} < U_{SC\text{-}2}$).

K_1 cannot work in ZVS mode. ε, which is introduced in (27), is set to 55 μs in the simulation system. Therefore, Δ and Γ can be

$$\begin{cases} \text{if } U_{SC-1} > U_{SC-2} : \Delta = 110\text{us}, \Gamma = 55\text{us} \\ \text{if } U_{SC-1} < U_{SC-2} : \Gamma = 110\text{us}, \Delta = 55\text{us} \end{cases} \tag{29}$$

The simulation results are shown in Fig. 14. u_{C1} and u_{C2} can both fall to 0, which means that K_1 and K_2 can work in ZVS mode. All the waveforms, such as the voltages and currents, coincide with the theoretical analysis in Fig. 8.

Fig. 15 shows a comparative picture of the voltages when the equalization system is either enabled or disabled. When the equalization system is disabled, the voltage difference considerably increases. When the equalization system is enabled, $U_{SC\text{-}2}$ decreases in a slow pace because the equalization system transfers the energy from $U_{SC\text{-}1}$ to $U_{SC\text{-}2}$ to keep the voltages equal. After about 0.95 s, the two voltages become equal (less than 0.2 V). The load of $U_{SC\text{-}2}$ is always larger than that of $U_{SC\text{-}1}$ in the whole process. Hence, the function of the equalization system is proved.

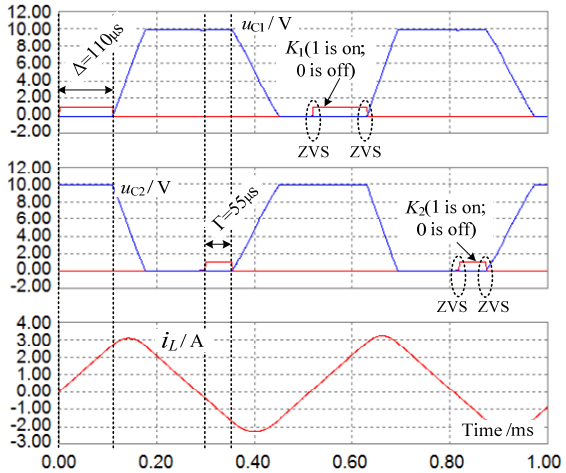

Fig. 14. Simulation results for module-1. (Δ = 110 μs, Γ = 55 μs when $U_{SC-1} > U_{SC-2}$; Δ = 55 μs, Γ = 110 μs when $U_{SC-1} < U_{SC-2}$).

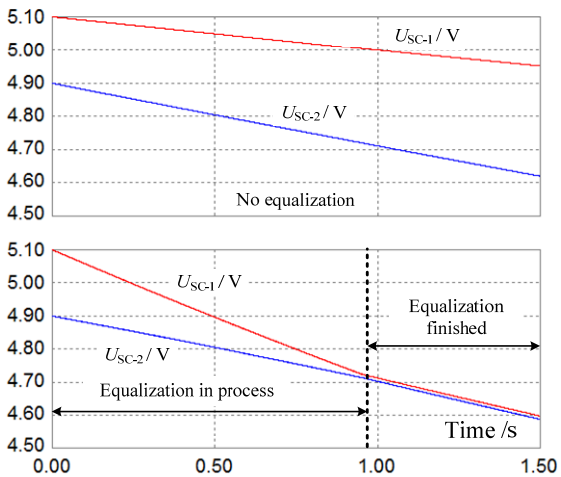

Fig. 15. Simulation results for SC cell voltages. (Δ = 110 μs, Γ = 55 μs when $U_{SC-1} > U_{SC-2}$; Δ = 55 μs, Γ = 110 μs when $U_{SC-1} < U_{SC-2}$).

V. Experimental Results

A. Two-cell Experimental System

A two-cell experimental system is built to verify the validity and correction of the proposed topology. Several 5.5 V/4 F super capacitors are adopted. The control algorithm is implemented in CPLD (EPM1270, by ALTERA) placed on the control board. The equalizer is placed on another board. The two boards are connected via a group of pins, as shown in Fig. 16.

In Fig. 16, two SC cells are connected in series. The equivalent capacitance of each SC cell is 3 × 4 F. A pre-charge resistor is connected in the circuit to limit the current flowing out of the AC/DC power module. The type of the two MOSFETs is 75NF75. The other parameters of the experimental system are shown in the photo.

The parameters obtained in (29) are also adopted in the experimental system. The power supply of the control board

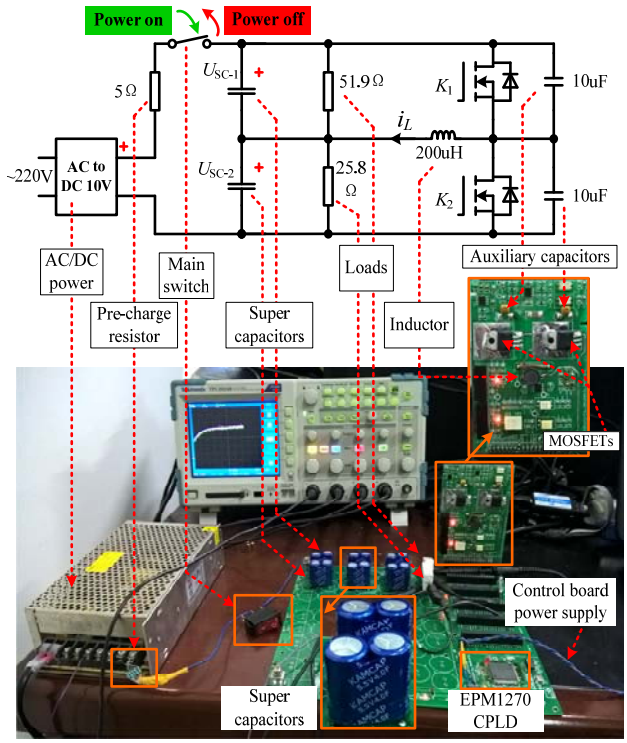

Fig. 16. Equivalent circuit and photo of the two-cell experimental system.

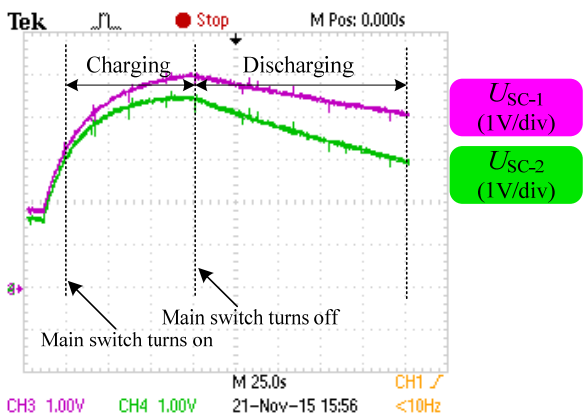

Fig. 17. Charging and discharging of the SC string without equalizers.

can be turned on or off. Thus, the equalization system can be enabled or disabled, and the comparative photos can be obtained.

The charging and discharging processes of an SC when the equalization system is disabled are shown in Fig. 17. As shown in Fig. 16, the string is charging when the main switch is on, whereas it is discharging when the main switch is off. In the whole process, U_{SC-1} is higher than U_{SC-2} because the loads are different (51.9 and 25.8 Ω, respectively).

Fig. 18 shows the experimental results when the equalization system is enabled. The two voltages are kept approximately equal in the charging and discharging processes.

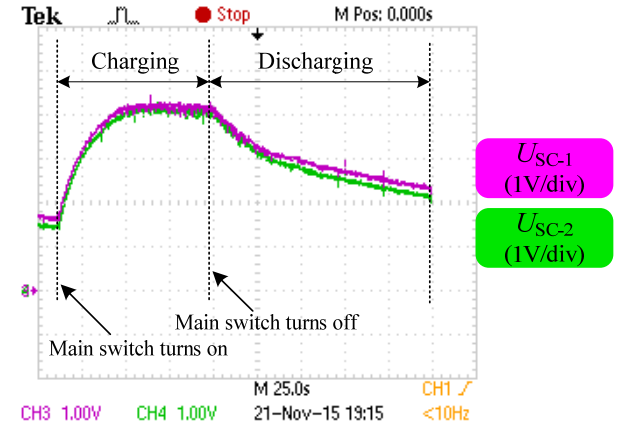

Fig. 18. Charging and discharging of the SC string with equalizers.

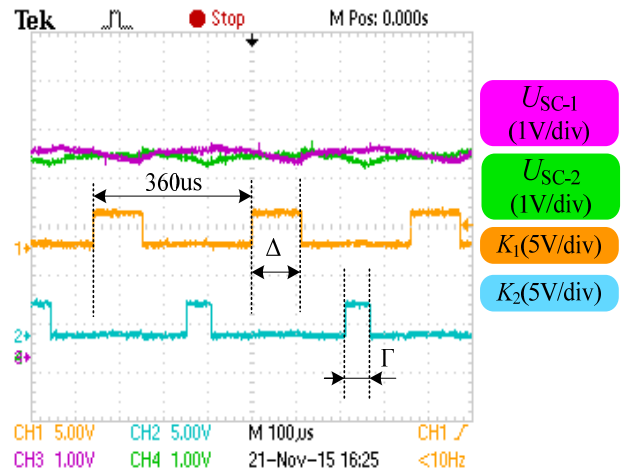

Fig. 19. SC voltages and gate signals.

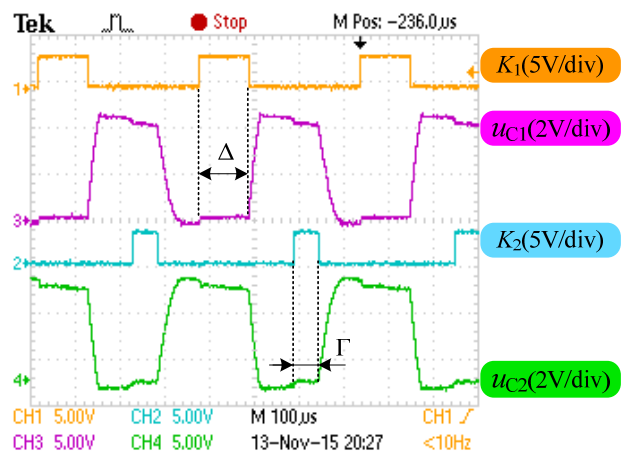

Fig. 20. Auxiliary capacitor voltages and gate signals.

Fig. 19 shows the gate signals for the two MOSFETs. In every cycle, Δ is 110 µs, and Γ is 55 µs. The two voltages are balanced because of the equalization system.

Fig. 20 shows the auxiliary capacitor voltages and gate signals of the MOSFETs. Obviously, the switches can work in ZVS mode.

As shown in Fig. 21, i_L rises when K_1 is turned on, and i_L drops when K_1 is turned off. The positive peak value of i_L is about 3 A, which is limited by Δ and the circuit parameters.

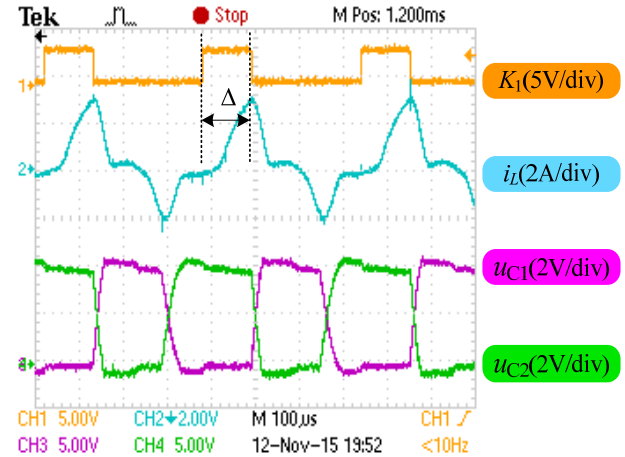

Fig. 21. Auxiliary capacitor voltages, inductor current, and gate signals.

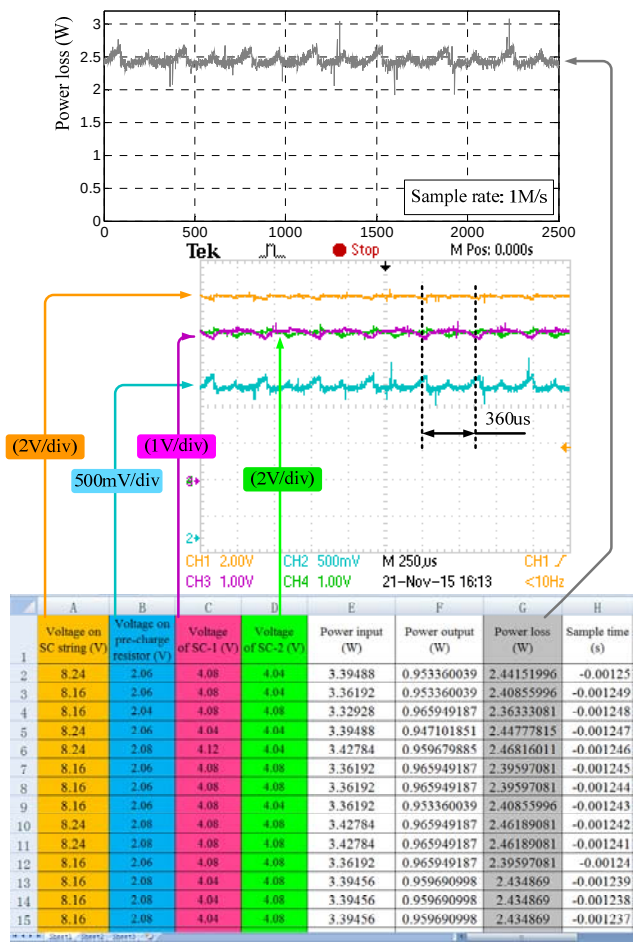

	A	B	C	D	E	F	G	H
1	Voltage on SC string (V)	Voltage on pre-charge resistor (V)	Voltage of SC-1 (V)	Voltage of SC-2 (V)	Power input (W)	Power output (W)	Power loss (W)	Sample time (s)
2	8.24	2.06	4.08	4.04	3.39488	0.953360039	2.44151996	-0.00125
3	8.16	2.06	4.08	4.04	3.36192	0.953360039	2.40855996	-0.001249
4	8.16	2.04	4.08	4.08	3.32928	0.965949187	2.36333081	-0.001248
5	8.24	2.06	4.04	4.04	3.39488	0.947101851	2.44777815	-0.001247
6	8.24	2.08	4.12	4.04	3.42784	0.959679885	2.46816011	-0.001246
7	8.16	2.06	4.08	4.08	3.36192	0.965949187	2.39597081	-0.001245
8	8.16	2.06	4.08	4.08	3.36192	0.965949187	2.39597081	-0.001244
9	8.16	2.06	4.08	4.04	3.36192	0.953360039	2.40855996	-0.001243
10	8.24	2.08	4.08	4.08	3.42784	0.965949187	2.46189081	-0.001242
11	8.24	2.08	4.08	4.08	3.42784	0.965949187	2.46189081	-0.001241
12	8.16	2.06	4.08	4.08	3.36192	0.965949187	2.39597081	-0.00124
13	8.16	2.08	4.04	4.08	3.39456	0.959690998	2.434869	-0.001239
14	8.16	2.08	4.04	4.08	3.39456	0.959690998	2.434869	-0.001238
15	8.16	2.08	4.04	4.08	3.39456	0.959690998	2.434869	-0.001237

Fig. 22. Power loss in the experimental system. (Top) Power loss. (Middle) Voltages of SC string. (Bottom) Data and results.

The power loss in the experimental system can be measured in the following steps:

(1) Calculate the power flowing into the two-cell experimental system, denoted by P_{in}.

(2) Calculate the power consumed by the two resistors connected in parallel with SC-1 and SC-2, denoted by P_{out}.

(3) The power loss is P_{in}–P_{out}.

As shown in Fig. 22, the power loss in the equalization system is around 2.5 W. The efficiency of the system can be calculated as P_{out}/P_{in}, and generally, the power loss of the equalizer is not larger than 2.5 W. When P_{out} is large, the efficiency increases. According to the experimental results shown in Fig. 22 (P_{out} =1 W), the efficiency is about 29%. When P_{out} is 3.5 W, the efficiency is about 59%.

B. Hybrid Energy Storage Experimental System

A hybrid energy storage system (HESS) is built to validate the performance of the SC string with the equalization systems proposed in this work.

In the HESS, the battery is of high energy density, but the response is low. The SCs introduced can improve the dynamic characteristics of the system.

The prototype consists of two H-bridges. In one H-bridge, there is a 36 V battery on the DC bus. In the other H-bridge, a super capacitor string comprising 21 5.5 V/4 F SCs (3 in parallel, 7 in series) is installed on the DC bus. Thus, the equivalent capacitance of the super capacitor string is 1.7 F. The rating voltage of the string is 38.5 V.

The main control board is based on DSP (TMS320F28335) and CPLD (EPM1270). It supports as many as 15 H-bridges. The main control board and the H-bridge are connected via a cable comprising four pairs of twisted wires. These pairs correspond to the power supply for the control board in the H-bridge, the differential serial signals to the H-bridge, the differential serial signals from the H-bridge, and the DC bus voltage of the H-bridge. The output voltage of the HESS is u_{out}; u_{cap} is the output voltage of the H-bridge connected to the SC string.

As shown in Fig. 23, the HESS can be connected to the power grid, motors, and electric vehicles to release or absorb energy and thereby reduce energy consumption while improving system reliability. For example, the HESS can be connected to the power grid and function as an active/reactive power regulator.

In Fig. 23, g_1–g_8 are the gate signals of the MOSFETs in the two H-bridges. These signals can be generated with a modified PWM method shown in Fig. 24.

As shown in Fig. 24, the peak value of u_{H1} is equal to the battery voltage in the H-bridge, and the peak value of u_{H2} is equal to the SC string voltage. When the HESS discharges, the voltage of the SC string drops, as shown in Fig. 24(a). By contrast, when the HESS is charging, the voltage of the SC string increases, as shown in Fig. 24(b). The gate signals in the two H-bridges can be generated as

$$g_1 = \text{not } g_2 = \begin{cases} \text{on}, & \text{if } |u_{ref}| \geq u_{H1} \\ \text{off}, & \text{if } |u_{ref}| < u_{H1} \end{cases} \quad (30)$$

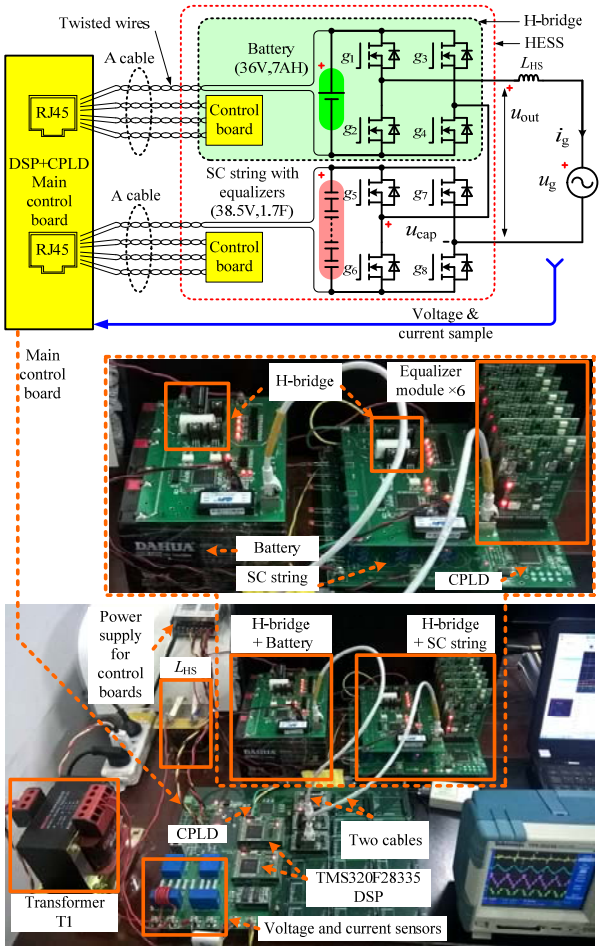

Fig. 23. Topology and photo of the HESS.

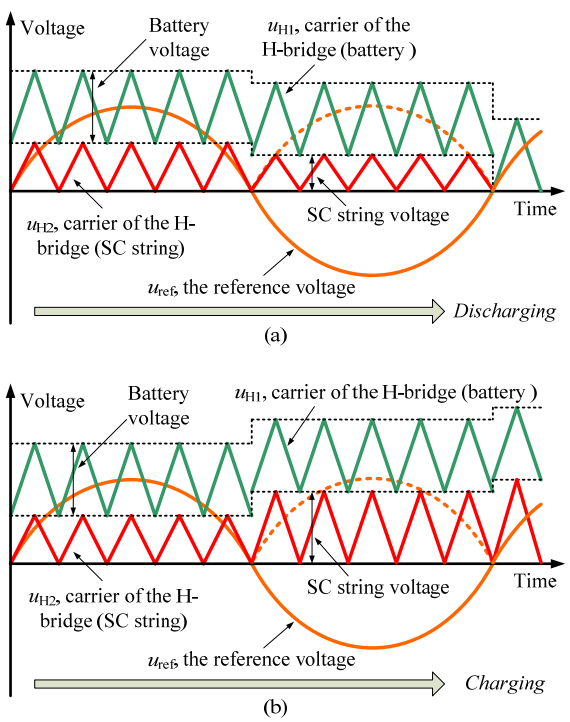

Fig. 24. Carriers and reference voltages when charging and discharging in the HESS.

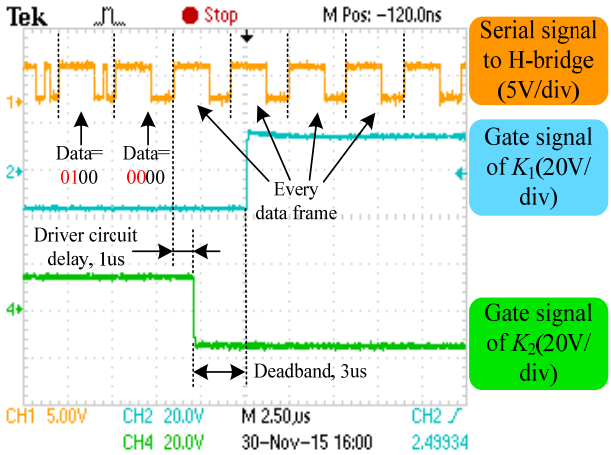

Fig. 25. Serial signal and gate signals.

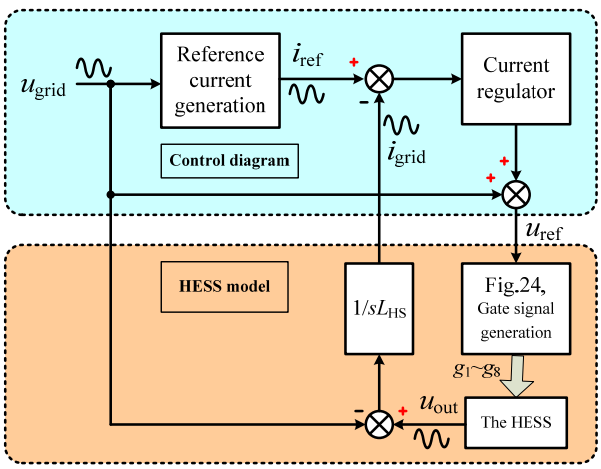

Fig. 26. Control diagram of the HESS.

TABLE III
PARAMETERS OF THE EXPERIMENTAL SYSTEM

Name	Value
T1	220 V/18 V, 50 Hz, 500 VA
L_{HS}	1 mH
Carrier (u_{H1}) frequency	5 kHz
Carrier (u_{H2}) frequency	5 kHz
Battery	36 V, 7 AH
SC cell parameters	5.5 V, 4 F
Number of SC cells	21 (3 in parallel, 7 in series)
SC string parameters	38.5 V, 1.7 F
Number of modules	6

$$g_3 = \text{not } g_4 = \begin{cases} \text{on}, & \text{if } u_{ref} \geq 0 \\ \text{off}, & \text{if } u_{ref} < 0 \end{cases} \quad (31)$$

$$g_5 = \text{not } g_6 = \begin{cases} \text{on}, & \text{if } |u_{ref}| \geq u_{H2} \\ \text{off}, & \text{if } |u_{ref}| < u_{H2} \end{cases} \quad (32)$$

$$g_7 = \text{not } g_8 = \begin{cases} \text{on}, & \text{if } u_{ref} \geq 0 \\ \text{off}, & \text{if } u_{ref} < 0 \end{cases} \quad (33)$$

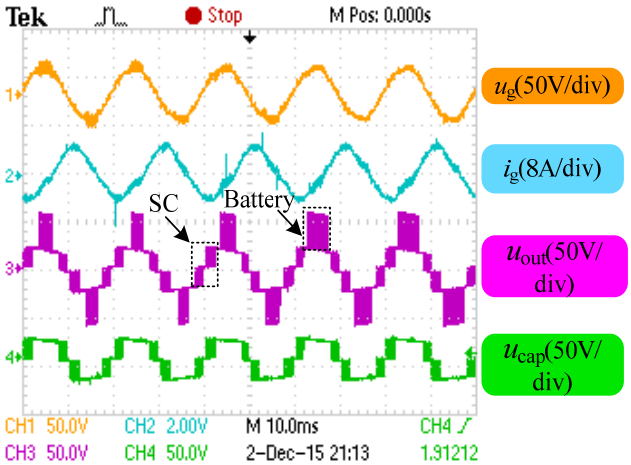

Fig. 27. Experimental results of the HESS when charging.

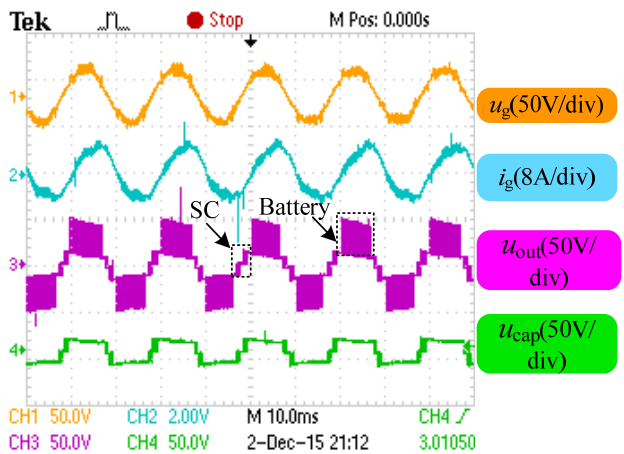

Fig. 28. Experimental results of the HESS when discharging.

The serial signal, which carries the gate signals and commands to the H-bridge, is shown in Fig. 25. Every data frame consists of seven idle bits, one start bit and, four data bits. The first two data bits indicate the gate signals for the H-bridge. The gate signals of K_1 and K_2 after decoding are shown in Fig. 25. The deadband is 3µs. Given the driver circuit, a 1 µs delay occurs.

The HESS is connected to the single-phase power grid through an inductor L_{HS}, as shown in Fig. 23. The control diagram is shown in Fig. 26. The reference current i_{ref} is generated on the basis of the charging or discharging state. A proportion current regulator is introduced to control the current flowing out. As discussed in [29], [30], the proportional current regulator cannot track sinusoidal signals with a zero steady-state error. Nevertheless, the charging and discharging for the HESS can be accomplished. Such process is enough to test the performance of the equalization system and control algorithm.

The parameters of the HESS are shown in Table III.

The voltage of the SC string is denoted by U_{SC}. In the experiment, 10 V ≤ U_{SC} ≤ 30 V. As shown in Fig. 27, when the HESS is charging, the angle between u_g and i_g is larger

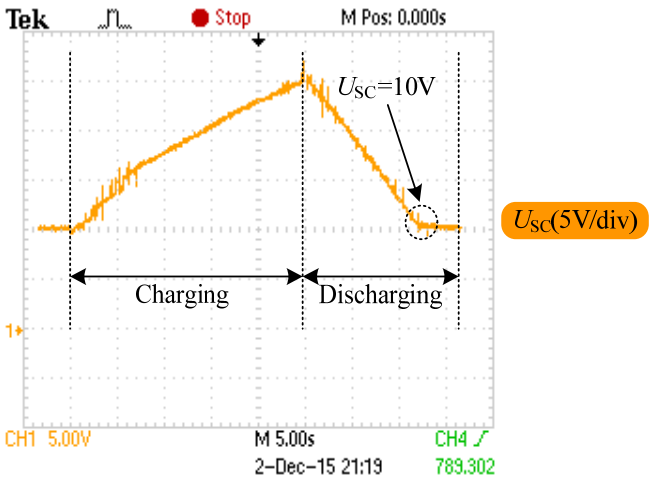

Fig. 29. Experimental results of the SC string voltage.

TABLE IV
SC CELL VOLTAGES IN THE HESS

Item	Test 1	Test 2	Test 3	Test 4
U_{SC-1} (V)	1.83	2.91	3.82	4.58
U_{SC-2} (V)	1.81	2.87	3.77	4.41
U_{SC-3} (V)	1.79	2.83	3.73	4.33
U_{SC-4} (V)	1.76	2.81	3.7	4.27
U_{SC-5} (V)	1.75	2.77	3.65	4.19
U_{SC-6} (V)	1.74	2.75	3.62	4.13
U_{SC-7} (V)	1.71	2.69	3.58	4.11
U_{SC} (V)	12.39	19.63	25.87	30.02
AVER (V)	1.77	2.80	3.70	4.29
MAX (V)	1.83	2.91	3.82	4.58
MIN (V)	1.71	2.69	3.58	4.11
MAX (%)	3.39	3.77	3.36	6.80
MIN (%)	−3.39	−4.08	−3.13	−4.16

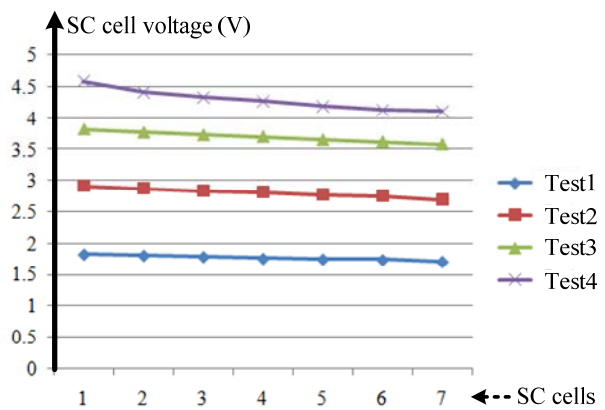

Fig. 30. Voltages of the SC cells in the HESS.

than 90 degrees. Moreover, u_{out} comprises five voltage levels, whereas u_{cap} comprises three voltage levels. When discharging, the angle between u_g and i_g is less than 90 degrees. The power flows from the HESS to the grid, as shown in Fig. 28. The experimental results for the charging and discharging processes coincide with those in Fig. 24.

The voltage of the SC string is shown in Fig. 29. In the charging stage, U_{SC} rises from 10 V to 25 V in 25 s. In the discharging stage, U_{SC} drops to 10 V in 12 s. Table IV shows the voltages of all the SC cells in the experiment. The maximal errors are 6.80% (positive) and 4.16% (negative), which indicate that the equalization system is practical. The voltages of the SC cells are depicted in Fig. 30. The cells are clearly balanced, and the SC string can work at the designed voltage level.

VI. CONCLUSION

The different characteristics of SC cells necessitate the installation of equalizers on SC strings to achieve balanced voltages. Equalizers should meet certain requirements, such as high efficiency, high modularity, and ease of control. This work proposes a topology for an equalizer based on a half-bridge inverter, an inductor, and two auxiliary capacitors. The inductor and auxiliary capacitors can make the switches work in ZVS mode and thereby reduce power losses and improve system efficiency. The equalizers can transfer energy between every two adjacent SC cells and make the voltages balanced. The working schemes and characteristics of the switches are discussed. The conditions for ZVS are proposed, and two key variables Δ and Γ are employed to indicate the switching patterns of the equalization system. A digital processor-based control algorithm that is inexpensive and easy to implement is proposed. The equalizer is highly modularized and can be used in SC strings regardless of the number of cells. Typically, for a string with N SC cells, the number of equalizer modules is $N-1$. The resistance of the circuit is considered, and it is found to cause the failure of ZVS. The reason is explained in this work, and a modified control method is given. The simulation results show that the analysis is correct and that the control method is effective.

A two-cell experimental system is established to test the equalizer module and measure system power losses. The results indicate that the equalizer can balance voltages under unbalanced load conditions. Moreover, the maximal power loss of the equalizer is about 2.5 W.

An HESS is built to estimate the performance of the equalization system with six equalizer modules. Batteries and SCs are utilized to store the energy from the power grid. The battery is of high power density, but the response is low. The SC string can charge and discharge quickly. The combination of batteries and SCs works well in the storage system. The charging and discharging performance of the HESS is tested. The SC string, which is made up of seven 5.5 V/12 F SC cells, can work at the designed voltage levels.

The topologies and theoretical analysis are validated by the simulation and experimental results. The equalizer can also be used in other types of strings, such as battery strings and fuel-cell strings.

ACKNOWLEDGMENT

This research work was supported by the National Natural Science Foundation of China (51207010).

REFERENCES

[1] W. G. Hurley, Y. S. Wong, and W. H. Wolfle, "Self-equalization of cell voltages to prolong the life of VRLA batteries in standby applications," *IEEE Trans*. *Ind*. *Electron*., Vol. 56, No. 6, pp. 2115-2120, Jun. 2009.

[2] L. Maharjan, S. Inoue, H. Akagi, and J. Askura, "State-of-charge (SOC)-balancing control of a battery energy storage system based on a cascaded PWM converter," *IEEE Trans*. *Power Electron*., Vol. 24, No. 6, Jun. 2009.

[3] L. Maharjan, T. Yamagishi, H. Akagi, and J. Asakura, "Fault-tolerant operation of a battery-energy-storage system based on a multilvel cascaded PWM converter with star configuration," *IEEE Trans*. *Power Electron*., Vol. 25, No. 9 pp. 2386-2396, Sep. 2010.

[4] L. Maharjan, T. Yamagishi, and H. Akagi, "Active-power control of individual converter cells for a battery energy storage system based on a multilevel cascaded PWM converter," *IEEE Trans*. *Power Electron*., Vol. 27, No. 3 pp. 1099-1107, Mar. 2012.

[5] H. Qian, J. Zhang, J. S. Lai, and W. Yu, "A high-efficiency grid-tie battery energy storage system," *IEEE Trans*. *Power Electron*., Vol. 26, No. 3, pp. 886-896, Mar. 2011.

[6] M. Bragard, N. Soltau, S. Thomas, and R. W. De Doncker, "The balance of renewable sources and user demands in grids: power electronics for modular battery energy storage systems," *IEEE Trans*. *Power Electron*., Vol. 25, No. 12, pp. 3049-3056, Dec. 2010.

[7] K. Sun, L. Zhang, Y. Xing, and J. M. Guerrero, "A distributed control strategy based on DC bus signaling for modular photovoltaic generation systems with battery energy storage," *IEEE Trans*. *Power Electron*., Vol. 26, No. 10, pp. 3032-3045, Oct. 2011.

[8] C. M. Young, N. Y. Chu, L. R. Chen, Y. C. Hsiao, and C. Z. Li, "A single-phase multilevel inverter with battery balancing," *IEEE Trans*. *Ind*. *Electron*., Vol. 60, No. 5, pp. 1972-1978, May 2013.

[9] N. H. Kutkut, H. L. N. Wiegman, D. M. Divan, and D. W. Novotny, "Design considerations for charge equalization of an electric vehicle," *IEEE Trans*. *Ind*. *Appl*., Vol. 35, No. 1, pp. 28-35, Jan./Feb. 1999.

[10] W. Dunham, M. Goldstein, and D. J. Kovensky, "A proposed use of zener diodes to improve satellite battery reliability," *Proceedings of the IEEE*, Vol. 51, No.3, pp. 514, Mar. 1963.

[11] H. S. Park, C. E. Kim, C. H. Kim, G. W. Moon, and J. H. Lee, "A modularized charge equalizer for an HEV lithium-ion battery string," *IEEE Trans*. *Ind*. *Electron*., Vol. 56, No. 5, pp. 1464-1476, May 2009.

[12] D. Y. Jung, Y. H. Kim, S. W. Kim, and S. H. Lee, "Development of ultracapacitor modules for 42-V automative electrical systems," *Journal of Power Sources*, Vol. 114, No. 2, pp. 366-373, Mar. 2003.

[13] S. H. Park, K. B. Park, H. S. Kim, G. W. Moon, and M. J. Youn, "Single-magnetic cell-to-cell charge equalization converter with reduced number of transformer windings," *IEEE Trans*. *Power Electron*., Vol. 27, No. 6, pp. 2900-2911, Jun. 2012.

[14] A. Xu, S. Xie, and X. Liu, "Dynamic voltage equalization for series-connected ultracapacitors in EV/HEV applications," *IEEE Trans*. *Veh. Technol.*, Vol. 58, No. 8, pp. 3981-3987, Oct. 2009.

[15] C. Karnjanapiboon, K. Jirasereeamornkul, and V. Monyakul, "High efficiency battery management system for serially connected battery string," in *IEEE International Symposium on Industrial Electronics*, pp. 1504-1509, Jul. 2009.

[16] C. H. Kim, M. Y. Kim, H. S. Park, and G. W. Moon, "A modularized two-stage charge equalizer with cell selection switches for series-connected lithium-ion battery string in an HEV," *IEEE Trans*. *Power Electron*., Vol. 27, No. 8, pp. 3764-3774, Aug. 2012.

[17] L. A. Tolbert, F. Z. Peng, T. Cunnyngham, and J. N. Chiasson, "Charge balance control schemes for cascade multilevel converter in hybrid electric vehicles," *IEEE Trans*. *Ind*. *Electron*., Vol. 49, No. 5, pp. 1058-1064, Oct. 2002.

[18] Y. Hinago and H. Koizumi, "A single-phase multilevel inverter using switched series/parallel DC voltage sources," *IEEE Trans. Ind. Electron.*, Vol. 57, No. 8, pp. 2643-2650, Aug. 2010.

[19] P. A. Cassani and S. S. Williamson, "Feasibility analysis of a novel cell equalizer topology for plug-in hybrid electric vehicle energy-storage systems," *IEEE Trans*. *Veh. Technol.*, Vol. 58, No. 8, pp. 3938-3946, Oct. 2009.

[20] P. A. Cassani and S. S. Williamson, "Design, testing, and validation of a simplified control scheme for a novel plug-in hybrid electric vehicle battery cell equalizer," *IEEE Trans*. *Ind. Electron*., Vol. 57, No. 12, pp. 3956-3962, Dec. 2010.

[21] L. F. Lavado Villa, T. P. Ho, J. C. Crebier, and B. Raison, "A power electronics equalizer application for partially shaded photovoltaic modules," *IEEE Trans*. *Ind. Electron*., Vol. 60, No. 3, pp. 1179-1190, Mar. 2013.

[22] M. Uno and K. Tanaka, "Influence of high-frequency charge-discharge cycling induced by cell voltage equalizers on the life performance of lithium-ion cells," *IEEE Trans*. *Veh. Technol.*, Vol. 60, No. 4, pp. 1505-1515, May 2011.

[23] A. C. Baughman and M. Ferdowsi, "Double-tiered switched-capacitor battery charge equalization technique," *IEEE Trans*. *Ind. Electron*., Vol. 55, No. 6, pp. 2277-2285, Jun. 2008.

[24] Y. S. Lee and M. W. Cheng, "Intelligent control battery equalization for series connected lithium-ion battery strings," *IEEE Trans*. *Ind. Electron*., Vol. 52, No. 5, pp. 1297-1307, Oct. 2005.

[25] Y. S. Lee and G. T. Cheng, "Quasi-resonant zero-current-switching bidirectional converter for battery equalization applications," *IEEE Trans*. *Power Electron*., Vol. 21, No. 5, pp. 1213-1224, Sep. 2006.

[26] Y. Yuanmao, K. W. E. Cheng, and Y. P. B. Yeung, "Zero-current switching switched-capacitor zero-voltage-gap automatic equalization system for series battery string," *IEEE Trans*. *Power Electron*., Vol. 27, No. 7, pp. 3234-3242, Jul. 2012.

[27] M. Uno and K. Tanaka, "Double-switch single-transformer cell voltage equalizer using a half-bridge inverter and a voltage multiplier for series-connected supercapacitors," *IEEE Trans*. *Veh. Technol.*, Vol. 61, No. 9, pp. 3920-3930, Nov. 2012.

[28] H. S. Park, C. H. Kim, K. B. Park, G. W. Moon, and J. H. Lee, "Design of a charge equalizer based on battery modularization," *IEEE Trans*. *Veh. Technol.*, Vol. 58, No. 7, pp. 3216-3223, Sep. 2009.
[29] A. G. Yepes, F. D. Freijedo, O. Lopez, and J. Doval-Gandoy, "Analysis and design of resonant current controllers for voltage-source converters by means of Nyquist diagrams and sensitivity function," *IEEE Trans. Ind. Electron.*, Vol. 58, No. 11, pp. 5231-5250, Nov. 2011.
[30] A. Timbus, M. Liserre, R. Teodorescu, P. Rodriguez, and F. Blaabjerg, "Evaluation of current controllers for distributed power generation systems," *IEEE Trans. Power Electron.*, Vol. 24, No. 3, pp. 654-664, Mar. 2009.

Zhigang Gao was born in Hebei Province, China. He received his B.S. degree from Tianjin University, Tianjin, China, in 2005; his M.S. degree in Electrical Engineering from the Institute of Electrical Engineering, Chinese Academy of Sciences, Beijing, China, in 2008; and his Ph.D. degree in Electrical Engineering from Tsinghua University, Beijing, China, in 2011. In 2011, he joined the School of Automation, Beijing Institute of Technology, Beijing, China, where he is presently working as a Lecturer. His current research interests include power systems, multilevel converters, motor drives, and renewable resource generation.

Fenlin Jiang was born in Shanxi Province, China. He received his B.S. degree in Electrical Engineering from the Shandong Jianzhu University, Shandong, China, in 2014. He is presently working toward his M.S. degree in the School of Automation, Beijing Institute of Technology, Beijing, China. His current research interests include power electronics, equalization technology, and energy storage systems.